Detection of a weak ring current in a nonaromatic porphyrin nanoring using magnetic circular dichroism

P. Kowalska,[a] M. D. Peeks,[b] T. Roliński,[a] H. L. Anderson,[b] and J. Waluk[a, c]

[a] *Institute of Physical Chemistry, Polish Academy of Sciences, Kasprzaka 44/52, 01-224, Warsaw, Poland;*[b] *Department of Chemistry, University of Oxford, Chemistry Research Laboratory, Oxford OX1 3TA, United Kingdom;* [c] *Faculty of Mathematics and Natural Sciences, College of Science, Cardinal Stefan Wyszyński University, Dewajtis 5, 01-815 Warsaw, Poland.*

Abstract

We compare the absorption and magnetic circular dichroism (MCD) spectra of a series of porphyrin oligomers – dimer, tetramer, and hexamer – bound in a linear or cyclic fashion. The MCD signal is extremely weak for low energy transitions in the linear oligomers, but it is amplified when the cyclic porphyrin hexamer binds a template, restricting rotational freedom. The appearance of Faraday *A* terms in the MCD spectra demonstrates the presence of magnetic moment, and thus, uncompensated electronic current. The value of the excited state magnetic moment estimated from the *A* term is very low compared with those of monomeric porphyrins, which confirms the nonaromatic character of the cyclic array and the lack of a global ring current in the ground state of the neutral nanoring. DFT calculations predict the absorption and MCD patterns reasonably well, but fail to reproduce the MCD sign inversion observed in substituted monomeric zinc porphyrins ("soft" chromophores). Interestingly, a correct sign pattern is predicted by INDO/S calculations. Analysis of the MCD spectra of the monomeric porphyrin unit allowed us to distinguish between two close-lying lowest energy transitions, which some previous assignments placed further apart. The present results prove the usefulness of MCD not only for deconvolution and assignment of electronic transitions, but also as a sensitive tool for detecting electronic ring currents.

Introduction

The electronic structure, spectra, and magnetic properties of porphyrins are strongly influenced by structural perturbations. These changes can be probed using various types of electronic spectroscopy. Among these techniques, magnetic circular dichroism (MCD) holds a special place, because of its very high sensitivity to minor structural variations. Porphyrins belong to the class of "soft MCD chromophores",[1] defined as compounds with similar values of the energy splitting between two highest occupied and two lowest unoccupied π orbitals (ΔHOMO and ΔLUMO, respectively). Depending on the type and position of substituents, the orbital splittings may be perturbed, resulting in ΔHOMO < ΔLUMO or ΔHOMO > ΔLUMO. In both cases, this leads to an increase of the relative absorption intensity of low energy Q electronic transitions with respect to the higher-lying Soret bands. Much more spectacular changes are observed in the MCD spectra: not only the intensities, but also the signs of the MCD signals may be reversed. Both "normal" (–, + sign sequence with increasing energy) and "inverted" MCD patterns have been reported for numerous porphyrins, their N-confused and reduced forms, chlorins, bacteriochlorins, isobacteriochlorins, corroles, norcorrole, phthalocyanines, and subporphyrins.[2-24]

The theory of MCD is quite complex[25] and involves electric and magnetic coupling between all the electronic states. However, a simple perimeter model developed by Michl,[26-28] based on Gouterman's four-orbital approach[29, 30] is able to satisfactorily explain the observed trends in electronic absorption and MCD spectra of π electron systems, both aromatic ($4N$+2 electrons)[1, 31, 32] and nonaromatic ($4N$ electrons).[31-35] For instance, it has been successfully applied to elucidate differences in absorption and MCD

spectra of porphyrin isomers: porphycene,[36] corrphycene,[37] and hemiporphycene.[38] The perimeter model can also account for such counterintuitive effects as the decrease of the magnetic moment with the increasing area encircled by the perimeter, observed for cyclohexa-, cyclohepta-, and cyclooctapyrrole.[39]

For the purpose of this work, it may be helpful to recall the basics of MCD. In the absence of ground state degeneracy, the intensity of the MCD signal, i.e., magnetically induced difference between absorption of left and right circularly polarized light, is given by the Faraday *A* and *B* terms: $[\Theta]_M(\tilde{\nu}) = -21.3458\sum_i[A_i f_i(\tilde{\nu}) + B_i g_i(\tilde{\nu})]$. $[\Theta]_M$ is the magnetically induced molar ellipticity in units of $deg \cdot L \cdot m^{-1} \cdot mol^{-1} \cdot G^{-1}$, $f(\tilde{\nu})$ and $g(\tilde{\nu})$ are the line shape functions; the latter is the same as in absorption to a particular electronic state *i*, whereas $f(\tilde{\nu})$ has the shape of the derivative of $g(\tilde{\nu})$. The values of Faraday terms for a given transition are extracted from the MCD spectra by integration over the respective bands (more than one in the case when vibronic structure is observed). The *A* term is nonzero only when the excited state involved in the transition is degenerate; it is characterized by a derivative lineshape. The value of *A*, in combination with that of the transition dipole strength *D*, enables the excited state magnetic moment μ to be calculated using the formula: $\mu = -2A/D$.

The perimeter model provides a simple physical picture of the magnetic moment based on the orbital electronic current (Figure 1). In an ideal, unperturbed [*n*]-atom perimeter, all π orbitals except the lowest one (and the highest, if *n* is even) are doubly degenerate. In each degenerate pair, the electron current runs in a clockwise sense in one orbital and in the counterclockwise sense in the other. This leads to the opposite directions of the out-of-plane component of the magnetic moment associated with each

orbital. The analytical formula has been provided for $\mu(n, k)$, the value of magnetic moment in the orbital k of an [n]-atom perimeter.[40] The electronic excitation changes the orbital occupancies, and thus, if degenerate orbitals are involved, a magnetic moment may arise, since the electronic currents no longer compensate each other. Various scenarios are possible, depending on whether the electronic configurations responsible for a given excited state are "electronic current sense-preserving" or "sense-reversing". The conceptually simplest case is given when the electron jumps from a doubly degenerate to a nondegenerate orbital. There is no magnetic moment in the latter, so the total magnetic moment is given by the hole created by the uncompensated electron in the initially filled pair of orbitals. Such a situation occurs, for example, in the trisulfur trinitride anion, a 10-π-electron molecule based on [6]-atom perimeter. The experimentally obtained value of the magnetic moment of $S_3N_3^-$ in its lowest $^1\pi\pi^*$ state is in perfect agreement with the corresponding theoretical parameter, $\mu(6, 2)$: –0.98 vs. –1.06 Bohr magnetons, respectively.[40] This result shows that the perimeter model can be very useful in the description and interpretation of magnetic properties.

Figure 1

In this work, we use MCD to investigate the electronic structure and excited states of linear and cyclic porphyrin arrays[41, 42] (Figure 2). These molecules are of great potential in the studies of diverse phenomena, such as electron[43-45] and energy[46] transfer, exciton dynamics and electronic delocalization,[47, 48] characterization of vibrational and electronic coherences,[49] two-photon absorption,[50, 51] and quantum interferences.[52, 53]

In a recent paper, evidence for global nanoring currents was provided by NMR and DFT computational studies.[54] It was shown that the aromatic or antiaromatic character is

determined by the number of π electrons. For the neutral six-porphyrin nanoring, no net global ring current, and thus non-aromatic character, was observed in the ground state. In the present work we demonstrate that a weak ring-current can be detected in the excited state by MCD in a neutral nanoring, but only when the cyclic structure is bound to a template, which suppresses rotational freedom and induces high symmetry. We also discuss the differences in the electronic structure and spectra between porphyrin oligomers assembled in a linear or a cyclic fashion, changes caused by enlarging the number of porphyrin subunits, and spectral variations caused by conformational flexibility. In addition, we test the reliability of theoretical methods in predicting MCD patterns, which is a challenging task in the case of soft chromophores. Finally, we point out the advantages of using MCD for the detection of weak electron currents.

Figure 2

Results and discussion

Spectral studies

Figure 3 shows the electronic absorption and MCD spectra of the monomeric unit **P1** compared with those of zinc *meso*-tetraphenylporphyrin ZnTPP. The absorption spectra, typical for porphyrins, are quite similar for both compounds, except for an increase in intensity of the lowest energy Q-band in **P1**. This effect can be explained by the lower symmetry of the molecule, caused by different substituents at the opposite *meso* positions. A spectacular difference is observed in the MCD spectra. The Q transitions reveal opposite sign patterns in the two compounds, whereas in the Soret region the same sign sequence is observed. This phenomenon, reported for various, differently substituted porphyrins,[2-5, 55] can readily be

explained by the perimeter model, which predicts a possibility of MCD sign inversion for soft chromophores, i.e., molecules for which ΔHOMO ≈ ΔLUMO. According to the theory, the reversal should first occur for the Q bands, exactly as observed for **P1**. A much stronger structural perturbation is required to induce such a reversal in the Soret transitions.

Figure 3

The spectra of linear oligomers **P2**, **P4**, and **P6** (Figure 4) reveal certain trends correlated with the number of monomer units. A red shift of the Q band is observed, from 14160 cm^{-1} in **P2** to 13020 cm^{-1} in **P4**, and to 12670 cm^{-1} in **P6**.[56] The maximum of the Soret band is red-shifted by 570 cm^{-1} upon elongation from **P2** to **P4**. It remains at practically the same position in **P6**. The whole absorption and MCD spectra of **P4** and **P6** are very similar, except for the red shift of the Q band in the latter.

Figure 4

The structure of the MCD spectra is quite rich in the Soret region, indicating the presence of several electronic transitions. In the Q region, the MCD signal is extremely weak, below the detection limit of the instrument for the region up to 15000 cm^{-1} in **P4** and **P6**. The strongest, negative peak at 16100 cm^{-1} in **P2** and 15850 cm^{-1} in **P4** and **P6** corresponds to a transition that is barely seen in absorption.

Comparison of the spectra of linear **P6** and cyclic ***c*-P6** (Figures 4 and 5) does not reveal major differences for both absorption and MCD. In contrast, a major change in MCD is observed upon introducing the **T6** template into the cyclic structure. The MCD spectra of ***c*-P6** and ***c*-P6•T6** are dramatically different in the Q-band region (Figure 5). In particular, the signal observed below 13000 cm^{-1} is at least an order of magnitude stronger in the templated structure. Contrary to the behaviour of linear and ***c*-P6** oligomers, the

MCD signal of ***c*-P6•T6** exhibits comparable intensities in the Q and Soret regions. Moreover, the shape of the MCD bands corresponding to the three strong absorption bands observed between 11000 cm^{-1} and 13000 cm^{-1} (Figure S1) strongly suggests the presence of *A* terms, possible for degenerate states and thus, high symmetry. Because of significant band overlap, it is difficult to tell whether the transitions observed in the MCD spectrum for the Soret region are also dominated by *A* terms, but this seems unlikely, based on the comparison of the positions of maxima and minima of the absorption and MCD curves.

For molecules with close-lying excited states, it is often extremely difficult to distinguish between the real and pseudo-*A* terms, the latter arising as a result of overlap between two bands with opposite *B* terms. An independent argument for *A* term assignment in ***c*-P6•T6** comes from a recent work that allowed identification of electronic transitions in this molecule from the analysis of quantum coherences.[53] It was demonstrated that the upper two of the three bands lying between 11000 cm^{-1} and 13000 cm^{-1} correspond to two single electronic transitions, assigned to S_5 and S_6. No other transitions were detected in this region.

Figure 5

The absorption and MCD spectra of **T6**, shown in Figure S2, lie in the spectral region blue-shifted from the Soret and Q bands. MCD reveals the presence of three electronic transitions. DFT calculations predict many more transitions in this region (Table S6), but the simulated shape of the MCD spectrum is in fair agreement with experiment.

The value of the magnetic dipole moment in the electronically excited degenerate state is given by $\mu = -2A/D$, where A is the Faraday term and D is the dipole strength of the transition. The exact determination of μ was not possible because of the close proximity of several bands, overlap of several electronic transitions and vibronic bands and a complicated interplay of A and B terms (vide infra). However, values of μ ranging between 0.02 and 0.04 Bohr magnetons could be estimated for each of the three "fingers" observed in the low energy region of the absorption spectrum of ***c*-P6•T6**. These values are extremely small, two orders of magnitude lower than those reported for metalloporphyrins[57] and cyclohexa- cyclohepta-, and cyclooctapyrroles.[39]

The absorption spectrum of ***c*-P6•T6** is much more structured than that of untemplated ***c*-P6**. This difference can be explained by the conformational flexibility of ***c*-P6**, well-documented for the linear oligomers.[58-60] It has been shown that a broad distribution of twisted conformations exists, due to almost barrierless rotation around the butadiyne linkers.[61] However, a planar structure can be obtained by complexing an oligomer with a multidentate ligand. In order to check the influence of flexibility/rigidity on the MCD spectra, we carried out spectrophotometric titrations of **P2**, **P4**, and **P6** with **T6**, measuring both absorption and MCD at consecutive steps (Figure 6). The observed changes in absorption, as already reported before,[41, 62, 63] are dramatic: upon complexation, the most intense Soret peak decreases in intensity (in **P2**) or disappears completely (in **P4** and **P6**). In the low energy region, growth of a strong absorption band and narrowing of the spectrum is observed.

In the Soret region, the MCD spectra follow the changes in absorption. In contrast, they practically do not change in the Q region, remaining extremely weak. The only

change detectable for MCD in this region is the decrease of the peak at ca. 16000 cm^{-1}, the only peak that could be reliably measured in the non-complexed molecules.

Figure 6

These observations lead to the conclusion that the differences in MCD intensity in the Q region observed between ***c*-P6•T6** on one hand, and **P2**, **P4**, **P6**, and ***c*-P6** on the other, are not simply related to the conformational flexibility. Moreover, since the MCD activity is observed for ***c*-P6•T6**, but not for ***c*-P6**, a cyclic structure is required, but not sufficient to induce a measurable signal in this region. Conformational flexibility in untemplated ***c*-P6** results in a low-symmetry, disordered structure. Restriction of conformational flexibility by incorporation of template (in ***c*-P6**) delivers a high symmetry structure. It therefore appears that the main factor is the high symmetry of ***c*-P6•T6**, suggesting an important role of Faraday *A* terms, which are non-zero only in symmetric ***c*-P6•T6**. In order to assess the contributions of *A* and *B* terms, we performed DFT simulations of absorption and MCD spectra.

Calculations and excited state assignments

Previous theoretical studies have shown that DFT calculations correctly predict the pattern of MCD signs in parent, unsubstituted zinc porphyrin[64, 65] and in ZnTPP.[64, 66] It was therefore interesting whether the effect of "inverted" MCD observed upon passing from ZnTPP to **P1** (Figure 3) can also be reproduced. In addition, since the MCD signs in porphyrins may strongly depend on substituents, we wanted to check the reliability of using simplified structures in the simulations. Initial calculations were done using INDO/S. The "inverted" MCD pattern (+, -, -, +) was correctly reproduced for models of

P1 as long as they contained two phenyl and two ethynyl substitutents. The excited state and MCD patterns were practically the same when the ethynyl hydrogen was replaced by trimethylsilyl group. However, when the ethynyl group was substituted with methyl or hydrogen, the calculations incorrectly predicted a "normal" -, + sequence in the Q region. This was accompanied by the reversal of the sign of |ΔHOMO| - |ΔLUMO|, from negative to positive, once again proving the validity of the perimeter model. Next, the role of phenyl substituents was checked. Their removal led to the "normal" -, + sequence in the Q region and to |ΔHOMO| > |ΔLUMO|. One can therefore conclude that the presence of both, phenyl and ethynyl groups is required for reliable simulations of the MCD of **P1**.

DFT calculations, performed for ZnTPP and **P1** using the same basis set and functional (TZP/BP86D), yielded the same –,+ sign patterns for the Q and Soret transitions. Thus, they fail in the case of Q bands in **P1** (Figure S3). The reason is the inability to predict the reversal of the ΔHOMO – ΔLUMO sign. For both molecules, the calculated ΔHOMO value is larger than ΔLUMO. In a highly symmetric (D_{4h}) zinc porphyrin this relation is dictated by symmetry, because the LUMO pair is degenerate. For **P1**, analysis of the MCD spectra based on the perimeter model indicates that ΔHOMO < ΔLUMO. The ΔHOMO and ΔLUMO values calculated for **P1** using BP86 functional were 0.41 and 0.24 eV; with Statistical Averaging of different Orbital-dependent model Potentials (SAOP), we obtained 0.36 and 0.23 eV. These differences are very small, which explains the difficulty in correctly predicting the MCD sign. Interestingly, INDO/S yields the correct splitting pattern: 0.06 and 0.17 eV, respectively, and therefore the correct MCD sign sequence. One should note that in the case of a highly

symmetric molecule, the correct relationship ΔHOMO > ΔLUMO will always be obtained, since ΔLUMO = 0. Contrary to previous theoretical studies,[64] we used lower symmetry of ZnTPP, with phenyl rings twisted by ca. 60^{o} from the plane of the porphyrin macrocycle. Such structure of ZnTPP has been determined by X-ray[67] and supersonic jet studies.[68] Since in this case orbital degeneracy is no longer imposed by symmetry, correct prediction of MCD signs becomes more challenging.

For the Soret bands, ZnTPP and **P1** exhibit the same pattern, correctly reproduced by calculations. According to the perimeter model, this is to be expected, since a major perturbation is required to alter the sign sequence for the Soret transitions. Therefore, such pattern is rarely observed.[4]

The ordering of the Q and Soret transitions, no longer degenerate in **P1**, has been a subject of controversy. It was initially proposed that the lowest energy Q band (S_1 state) is short axis polarized (perpendicular to the acetylene groups)[51] based on comparison with similar porphyrins lacking meso-aryl groups,[49,50] however EPR magnetophotoselection experiments, supported by DFT calculations, demonstrated that this band is long axis polarized.[69] Our present calculations confirm this assignment. Importantly, the MCD spectrum measured for **P1** (Figure 3) clearly demonstrates that the S_1 and S_2 states lie very close to each other, less than 300 cm^{-1}. This result is in line with both TZP/BP86D and INDO/S calculations that predict an S_1-S_2 gap of 290 and 24 cm^{-1}, respectively. Therefore, the previous assignments[60, 70] that placed these states more than 1000 cm^{-1} apart should be corrected. As is often the case for porphyrin, the higher energy Q band can be assigned to a vibronic component, predominantly short axis polarized. Moreover, the excellent agreement between calculated and observed transition energies (in each case

the difference does not exceed 600 cm^{-1}) leads us to suggest that the lower energy transition in the Soret region is short-axis polarized.

As in the case of **P1**, initial calculations for oligomers were performed to check the sensitivity of calculated MCD signals on substituents. Using INDO/S, we compared the patterns obtained for simplified model systems for **P2**. First, two zinc porphyrins linked by a butadiyne bridge were considered. Next, two ethynyl groups, and, finally, four phenyl substituents were added. Planar structures were assumed, but we also checked the effect of 45 twisting of the two porphyrin rings. Very similar MCD patterns were obtained in all cases for the Q region. Regarding the higher energy range, introduction of phenyl substituents led to the appearance of strong transitions around 30000 cm^{-1}. Based on these results, we decided not to use phenyl substituents in the calculations. The terminal ethynyl rings, however, have been kept, to enable reliable comparison between **P6** and **c-P6**.

In order to understand the changes in the energy and intensity of absorption bands occurring when the monomeric units assemble into oligomers, one can analyse orbital energy shifts or, alternatively, use exciton coupling theory.[41, 71] In addition, the changes due to twisting should be taken into account. This has been extensively discussed in the literature, in particular for the dimers.[50, 58, 63, 72] Our present calculations agree well with the previous ones regarding the shapes of orbitals and their relative energies (Figures S4-S8), transition energies, and polarizations. The experimental and theoretical results are compared in Figure 7 for the planar form of **P2**. The calculations predict that the absorption is dominated by long-axis polarized transitions, particularly in the low energy region. Given the complexity of the experimental spectra and the assumptions made in

calculations (completely planar structure of D_{2h} symmetry), the agreement between measured and simulated spectra is quite good. This is also true for the calculated MCD pattern. We were rather pleasantly surprised to find that the calculations reproduce the complex MCD pattern extremely well, comprising five peaks in the region between 20000–25000 cm^{-1}. The transition energies in this region determined from MCD agree well with those reported using fluorescence anisotropy.[70]

Figure 7

The analysis of the measured and simulated spectra of linear tetramer **P4** and hexamer **P6** (Figures S9–S10) shows, in comparison with **P2**, an increasing number of strong, long axis (B_{3u}) polarized transitions, dominating in the low energy region. Also in the Soret region the overall intensity is predicted to be higher for transitions to B_{3u} than B_{1u} states, but the latter contribute much more than in the low energy range. The calculations predict over 130 B_{3u} and B_{2u} transitions (66 of each symmetry) to lie below 30000 cm^{-1} in **P4**. For **P6**, this number increases to 150+132 = 282. It would be risky, if not naive, to expect for such a case excellent agreement with experiment. Still, some general experimental features are well reproduced, such as (i) different absorption patterns for **P4** and **P6** in the Q region; (ii) very similar absorption of the two molecules in the higher energy range; (iii) very low MCD intensity for Q transitions; (iv) similar MCD shapes in the Soret region.

A recent paper described DFT and TDDFT calculations of electronic structure and spectra of 3D nanocage and nanobarrel structures built from tetraazaporphyrin and subtetraazaporphyrin units.[73] In several ways, the results of these calculations are similar to those reported here: (i) significant contributions of the linker atoms to frontier orbitals

was observed (cf. Figures S4-S8); (ii) shifts to low energy were predicted for the conjugated systems; (iii) large increase in the intensity of the low energy transitions in comparison with individual chromophores was obtained.

The results of calculations proved helpful in addressing the challenging issue of explaining the large difference between the linear and the cyclic, templated hexamer observed in MCD. To make the computations feasible, ***c*-P6•T6** was approximated by ***c*-P6**, assuming D_{6h} symmetry. Even then, the total number of calculated excited states lying below 30000 cm^{-1} was as large as 802. Of those, 173 transitions were allowed (2x69 of E_{1u} and 35 of A_{2u} symmetry). A reliable calculation of MCD terms requires that the number of electronic transitions considered is at least two times larger than the number of states for which the MCD spectrum is simulated. Therefore, the results obtained for the Soret region may be less reliable than those obtained for lower energy transitions. We focus on the latter, recalling that the differences between ***c*-P6•T6** and **P6** are observed exactly in this region (cf. Figures 4–5). Figure 8 shows the simulated absorption and MCD spectra of ***c*-P6**. In agreement with experiment, the calculated absorption is quite similar to that simulated for **P6** (Figure S10). Two strongly allowed transitions are predicted in the low energy range. They correspond to S_1 and S_4 in **P6** (B_{1u} symmetry) and to S_6 and S_{20} in ***c*-P6** (E_{1u} symmetry). A large number of other transitions of different symmetries is calculated in this region, e.g., a weakly allowed S_2 (E_{1u})) or forbidden S_1 (A_{2g}) in ***c*-P6**.

In contrast to the absorption and in full agreement with experiment, the simulated MCD patterns are completely different for the two systems. Instead of weak MCD activity in the low energy region calculated for **P4** and **P6** (Figures S9–S10), the

calculated MCD signal is predicted to be strong in "rigid" D_{6h} ***c*-P6**. Contributions from both *A* and *B* terms of allowed E_{1u} transitions are equally important (*A* terms are dominant for some transitions), and the resulting spectrum is the result of the interplay between the two. The final pattern of the simulated MCD spectrum: a weak positive signal followed by three negative and two positive peaks, agrees with experiment (Figure 4). It would, however, be too optimistic to claim that theory reproduces the experiment very well, since the measured spectra may contain vibronic contributions that are not taken into account in calculations. Still, one can safely conclude that the calculations confirmed the hypothesis that the origin of the much stronger MCD signal in ***c*-P6•T6** is the cyclic topology combined with high symmetry, induced by restricted rotational freedom. Moreover, a recent work devoted to identification of electronic transitions in ***c*-P6•T6** from the analysis of electronic and vibrational coherences suggests that at least the lower two of the three strong bands observed in the low energy range are not of vibrational, but of electronic origin.[53]

Figure 8

Summary

The results obtained for ***c*-P6•T6**, a π-conjugated non-aromatic macrocycle, demonstrate that magnetic circular dichroism is capable of detecting very weak electron currents and, in general, changes in the electronic structure and conformational equilibria which are difficult to monitor using such techniques as electronic absorption or NMR. This was demonstrated by spectacular differences in the MCD spectra of **P6**, ***c*-P6**, and ***c*-P6•T6**. In order to understand the origin of higher sensitivity of MCD vs. NMR when

investigating electron currents, one should realize that the latter technique probes the response to the magnetic field for ground state molecules, whereas MCD deals with electronically excited states. In the latter case, owing to the involvement of the orbitals which are empty in S_0 (and of the holes created by electrons promoted to higher orbitals), the magnetic field introduces imbalance between much larger electronic currents than for ground state molecules. This is especially true if the electronic transitions involve "sense reversing" configurations that lead to large magnetic moments. Such configurations are usually responsible for the low energy transitions, but contribute much less to the Soret bands. In fact, this may be one of the reasons why we observed *A* terms in the Q region.

While considering macrocyclic oligomers, one should note that, in addition to the current due to the whole nanoring, ring currents from porphyrin units may also contribute. By comparing the nanoring and non-nanoring structures, possessing the same number of porphyrin units, and characterized by the same templation mode, we are able to distinguish between single porphyrin and nanoring ring-currents.

A natural extension of this work would be the measurement of charged species, either aromatic (***c*-P6•T6**$^{6+}$) or antiaromatic (***c*-P6•T6**$^{4+}$). We plan to do such experiments, even though preliminary calculations and spectroelectrochemistry show that the lowest excited states occur at energies too low to lie within the available range of the spectropolarimeter.[74] The availability of such spectra could enable us to check whether the perimeter model can be extended to treat extremely large aromatic systems. Recent application of MCD for the analysis of in-plane aromaticity in cycloparaphenylene dications[32] seems to confirm such a possibility.

Acknowledgements

This work was partially supported by the Polish National Science Centre (NCN) through grants 2013/10/M/ST4/00069 and 2016/22/A/ST4/00029, the PL-Grid Infrastructure grant, the EPSRC and by the ERC (grant 320969).

Experimental and theoretical methods

The molecules were synthesized according to procedures described before.[56,75] Toluene (spectral grade, Uvasol, Merck), was used as solvent. The absorption spectra were recorded on a SHIMADZU UV-3100 spectrophotometer. The spectra are shown in the Figures in the units of absorption coefficient ε ($M^{-1}\cdot cm^{-1}$). The MCD spectra were measured on an OLIS DSM 17 spectropolarimeter equipped with a permanent magnet. The instrument was calibrated using aqueous solutions of $CoSO_4$ and D-camphorsulfonic acid. In order to increase the sensitivity in the near IR region, the original R955 photomultipliers were replaced with a pair of Hamamatsu R316 PMTs. 1 mm quartz cells were used, and the concentrations were adjusted to give the maximum optical density of about 1.0. The MCD spectra are always corrected for the baseline, which is recorded using the same cell filled with pure solvent. The spectra are presented in the units of molar ellipticity per unit magnetic field, $[\Theta]_M$ ($10^4\cdot deg\cdot M^{-1}\cdot m^{-1}\cdot T^{-1}$).

Titration of **P2**, **P4** and **P6** linear porphyrins with **T6** was carried out in toluene solutions. The concentration of porphyrins was determined spectrally on the basis of the absorption coefficients. The solution of **T6** was prepared by dissolving a known amount of the compound in toluene. Then, a specific amount of porphyrin solution was titrated using an automatic pipette according to the calculated molar ratio.

DFT calculations were performed with the Amsterdam Density Functional (ADF) package (version 2014.07),[76, 77] where the computation of MCD *A* and *B* terms based on time-dependent DFT has been implemented.[78-80] The BP86 functional[81, 82] was used, to enable comparison with previous calculations for porphyrins.[64] For **P1**, calculations employing the SAOP potential (Statistical Averaging of different Orbital-dependent model Potentials) were also carried out, yielding very similar results. The double zeta plus polarization (DZP) basis set was used; a larger basis set (TZP) was employed for **P1**, the smallest of the investigated molecules. Prior to calculating the absorption and MCD spectra, the geometries were optimized using the same functional and basis set. In some cases, specific symmetry was assumed, in order to obtain "idealized" planar or cyclic structures. This allows rational comparisons along the series and is important, given the role conformational flexibility plays in both, linear and cyclic oligomers.

We also used a home-written semiempirical INDO/S program. It was based on a version kindly provided by Josef Michl and John Downing (DZDO), and extended to enable calculations for zinc-containing molecules. In the CI procedure, singly excited configurations, involving 14 to 30 highest occupied and 14 to 30 lowest unoccupied orbitals were taken into account. The results obtained for different sizes of the CI base were compared to check the stability of calculated excited state parameters.

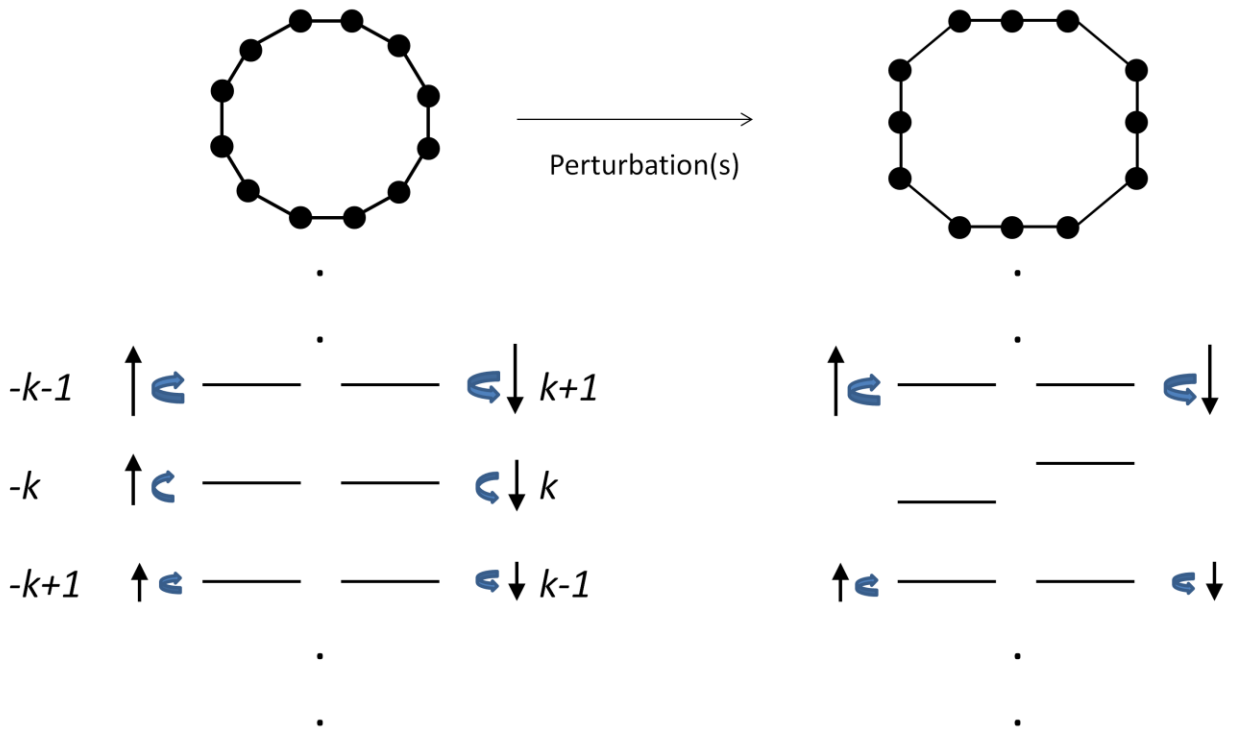

Figure 1. Schematic representation of orbitals, electron circulation and the resulting magnetic moments. Left: parent, high symmetry perimeter; *k* is the orbital number. Right: orbital energy scheme for a real molecule, modelled as a perturbed perimeter; some degeneracies are lost as a result of perturbation. The curved arrows show the sense and magnitude of electron currents. The vertical straight arrows indicate the direction and magnitude of the magnetic moment associated with each orbital. It was assumed that the perturbation preserves high symmetry, i.e. C_n, with $n \geq 3$; otherwise all the degeneracies would have been lost.

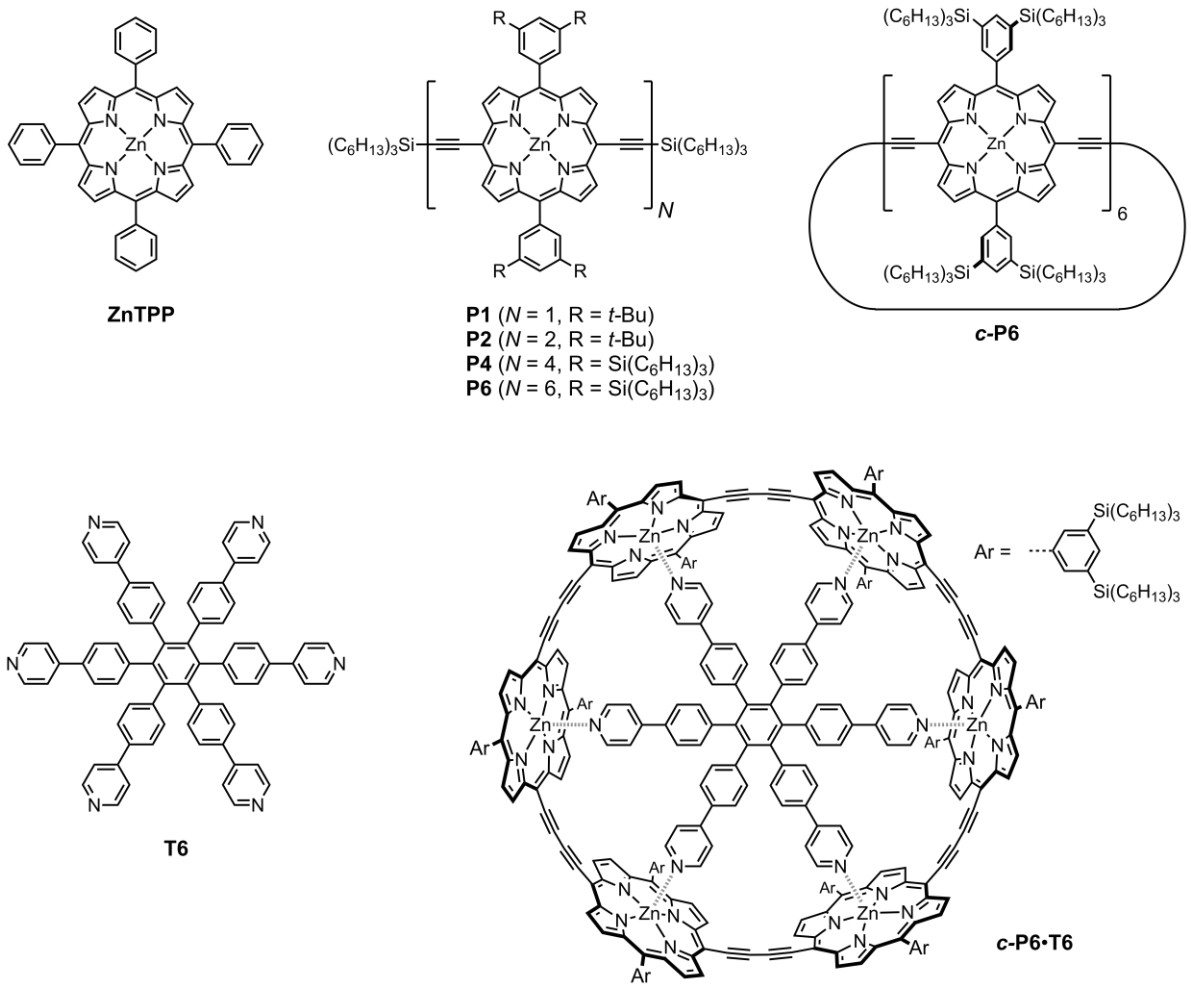

Figure 2. Chemical structures of the compounds used in this investigation.

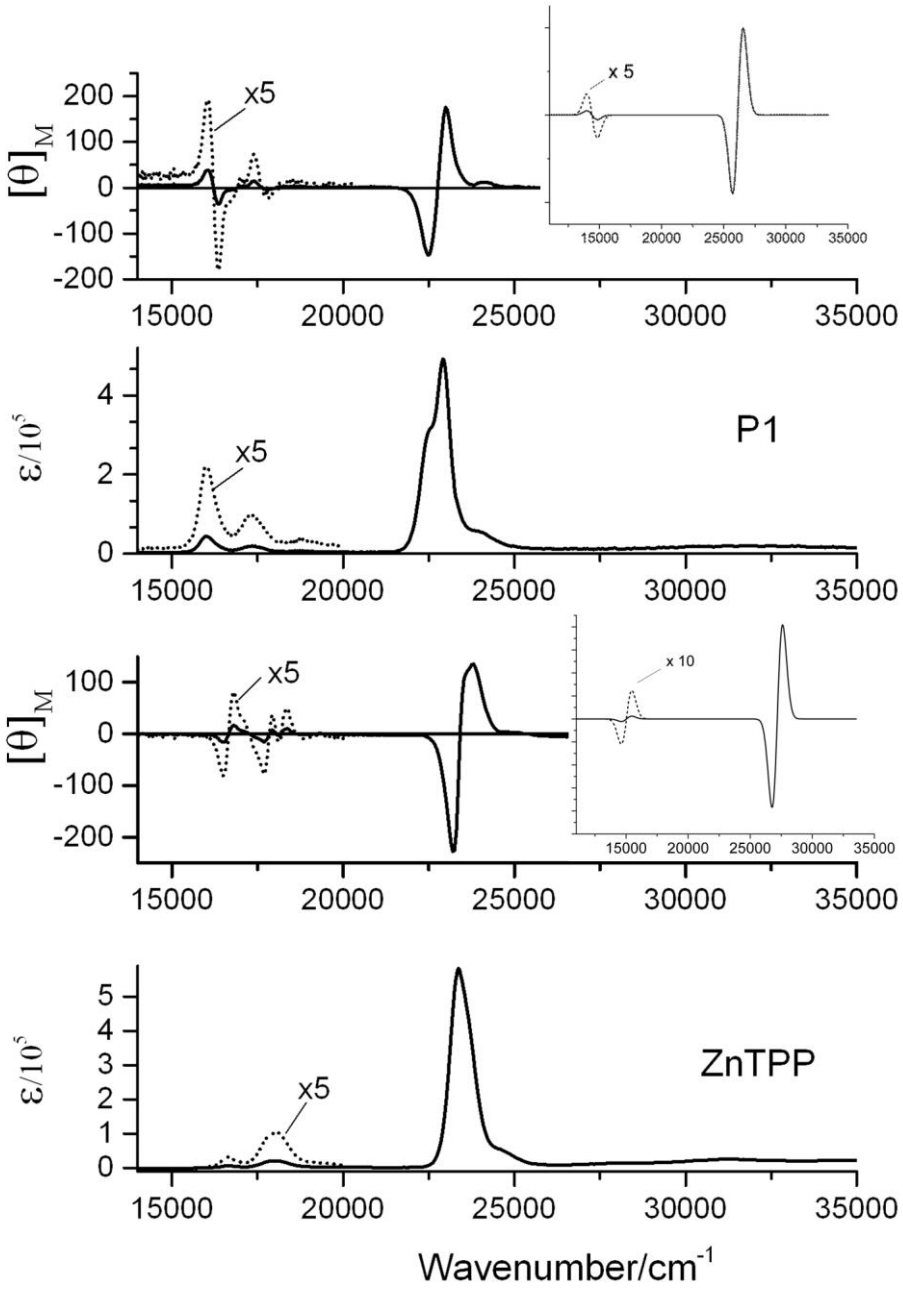

Figure 3. Absorption and MCD spectra of ZnTPP (bottom) and **P1** (top) measured in toluene at 293 K. Inserts, INDO/S simulated MCD signals (1000 cm^{-1} bandwidth was assumed).

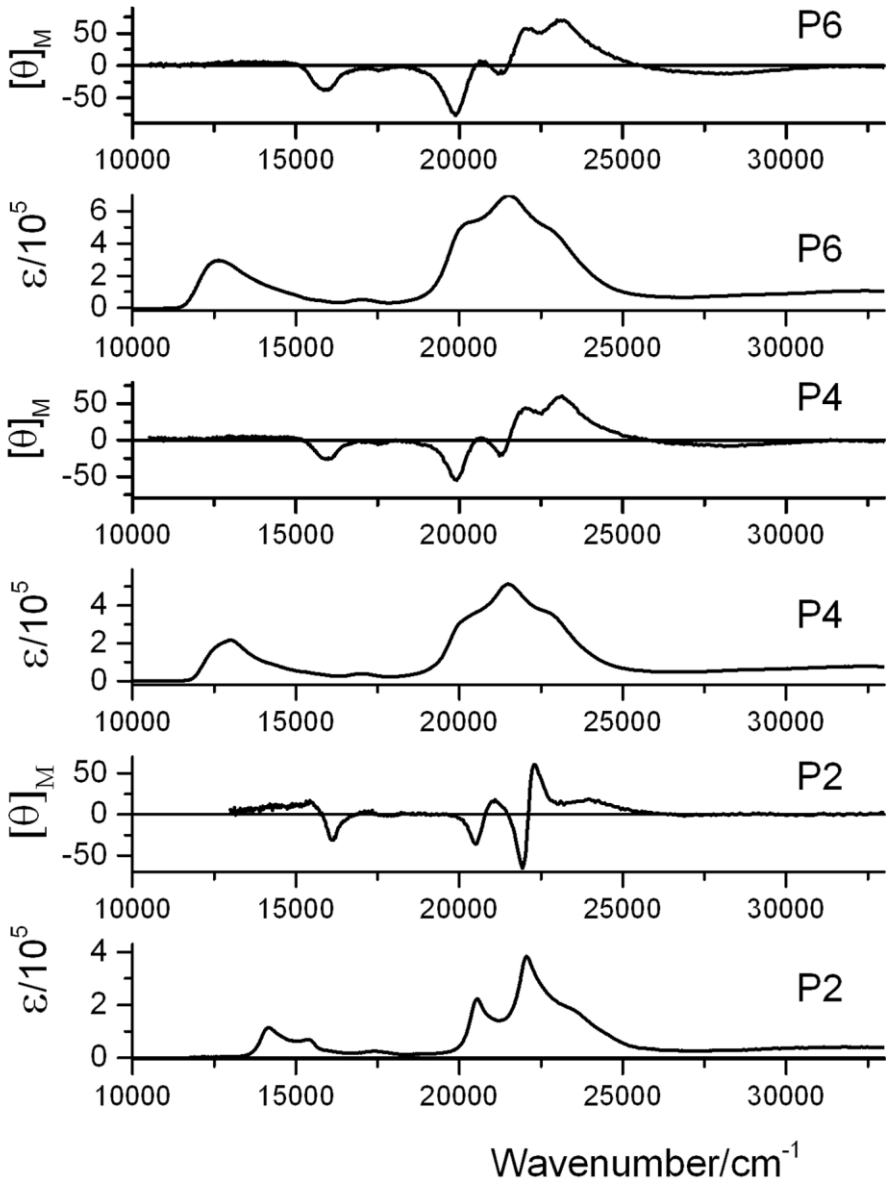

Figure 4. Absorption and MCD spectra of **P2** (bottom), **P4** (middle) and **P6** (top) measured in toluene at 293 K.

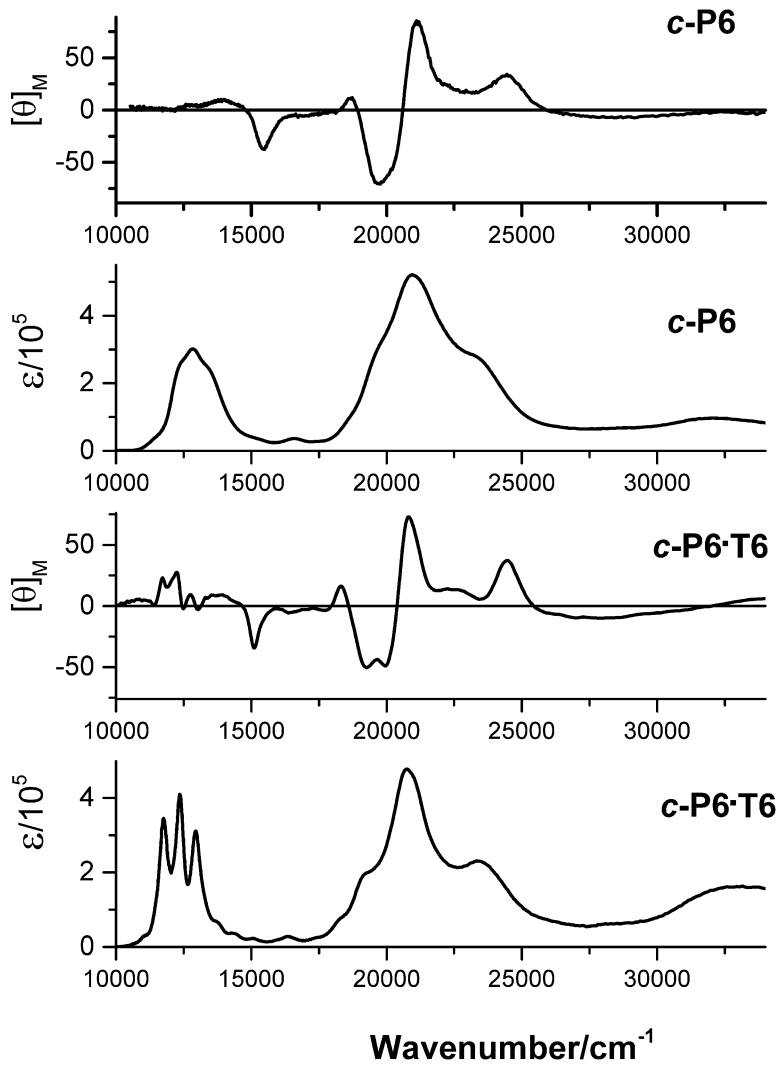

Figure 5. Absorption and MCD spectra of ***c*-P6•T6** (bottom) and ***c*-P6** (top) measured in toluene at 293 K.

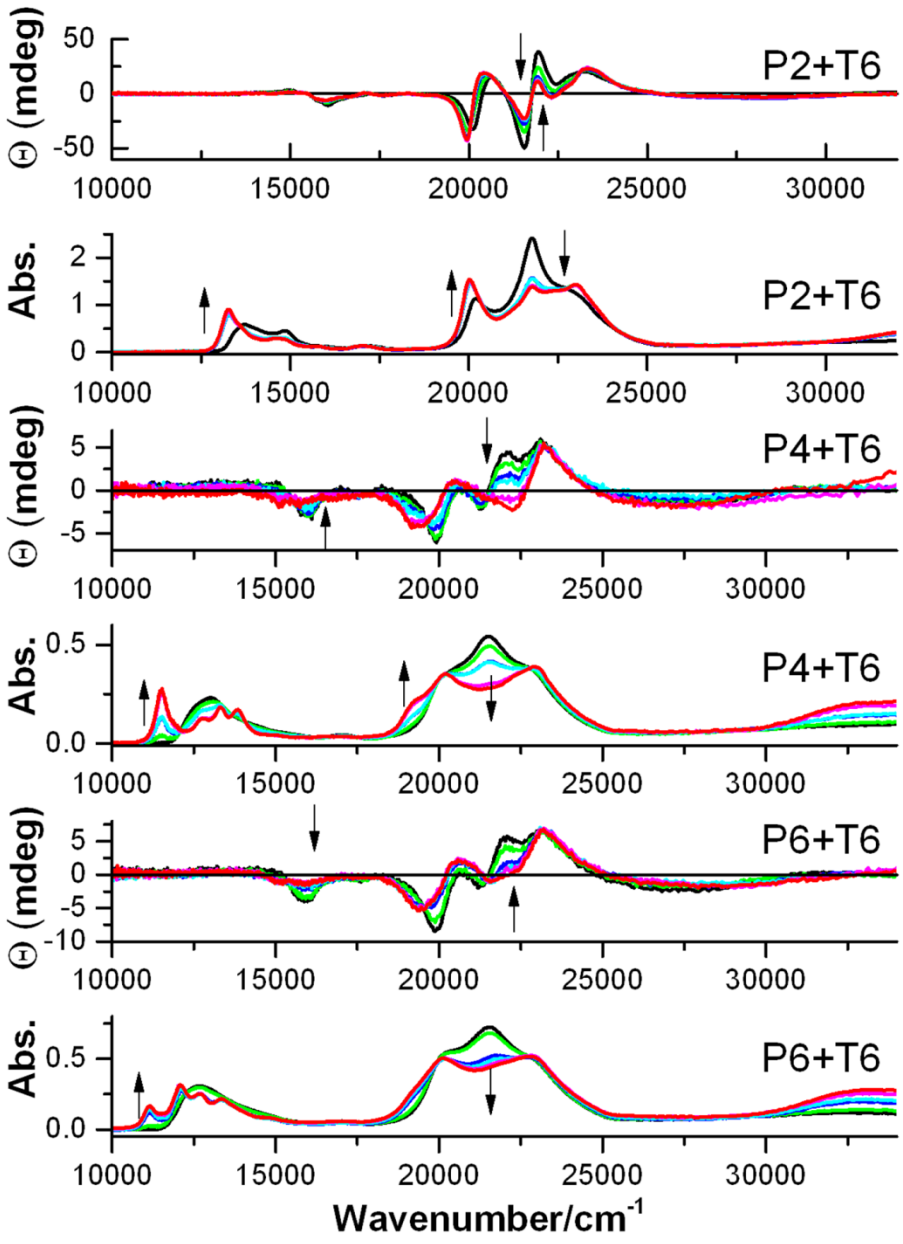

Figure 6. Changes in absorption and MCD spectra observed after adding **T6** to a solution of linear oligomer (0, 1, 2, 4, 5, and 6 equivalents for **P2**, 0, 2, 4, 5, and 8 for **P4**, and 0, 2, 3, and 8 for **P6**; because of slow complexation kinetics, some intermediate spectra were remeasured 24 hours after adding **T6**). The arrows show the direction of spectral changes upon adding **T6**. Top to bottom: **P2**, **P4**, and **P6**.

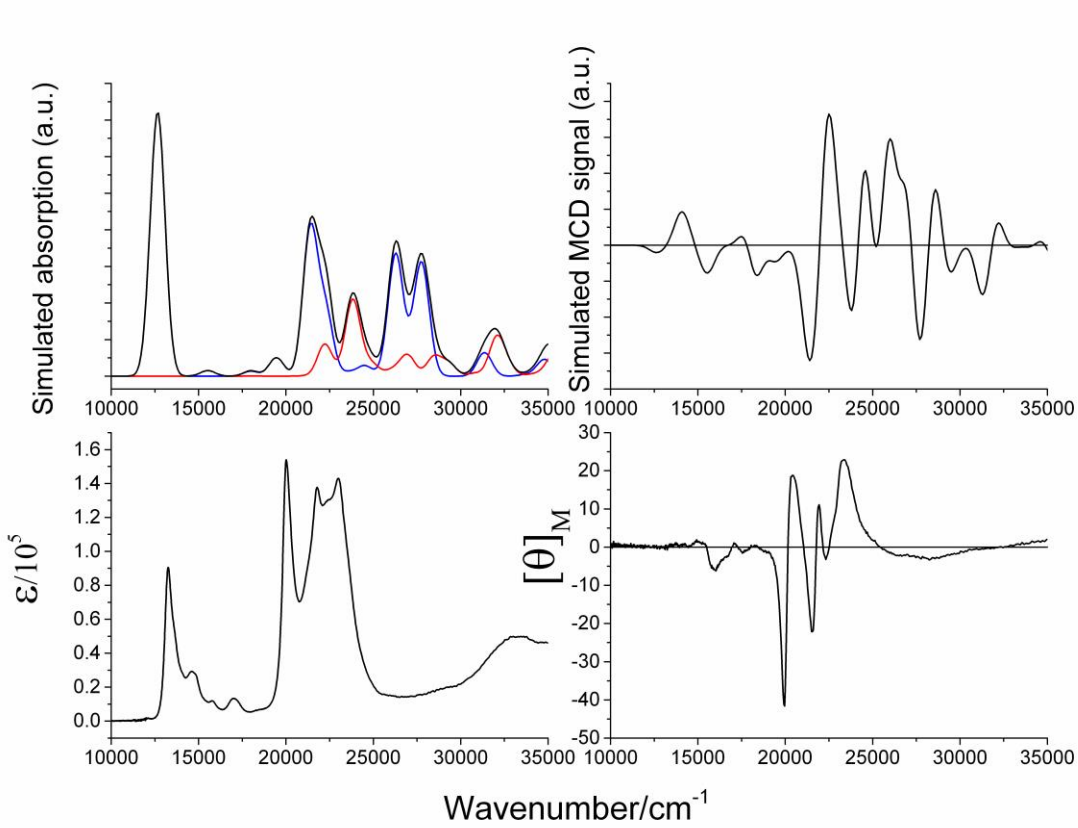

Figure 7. Experimental (bottom) and simulated (top) absorption and MCD spectra of planar **P2**. The simulated absorption spectrum (black) consists of long- and short-axis polarized components (blue and red, respectively). 1000 cm^{-1} bandwidth was assumed in the simulations. The experimental spectra are those obtained for **P2** complexed with **T6** (*cf.* Figure 6).

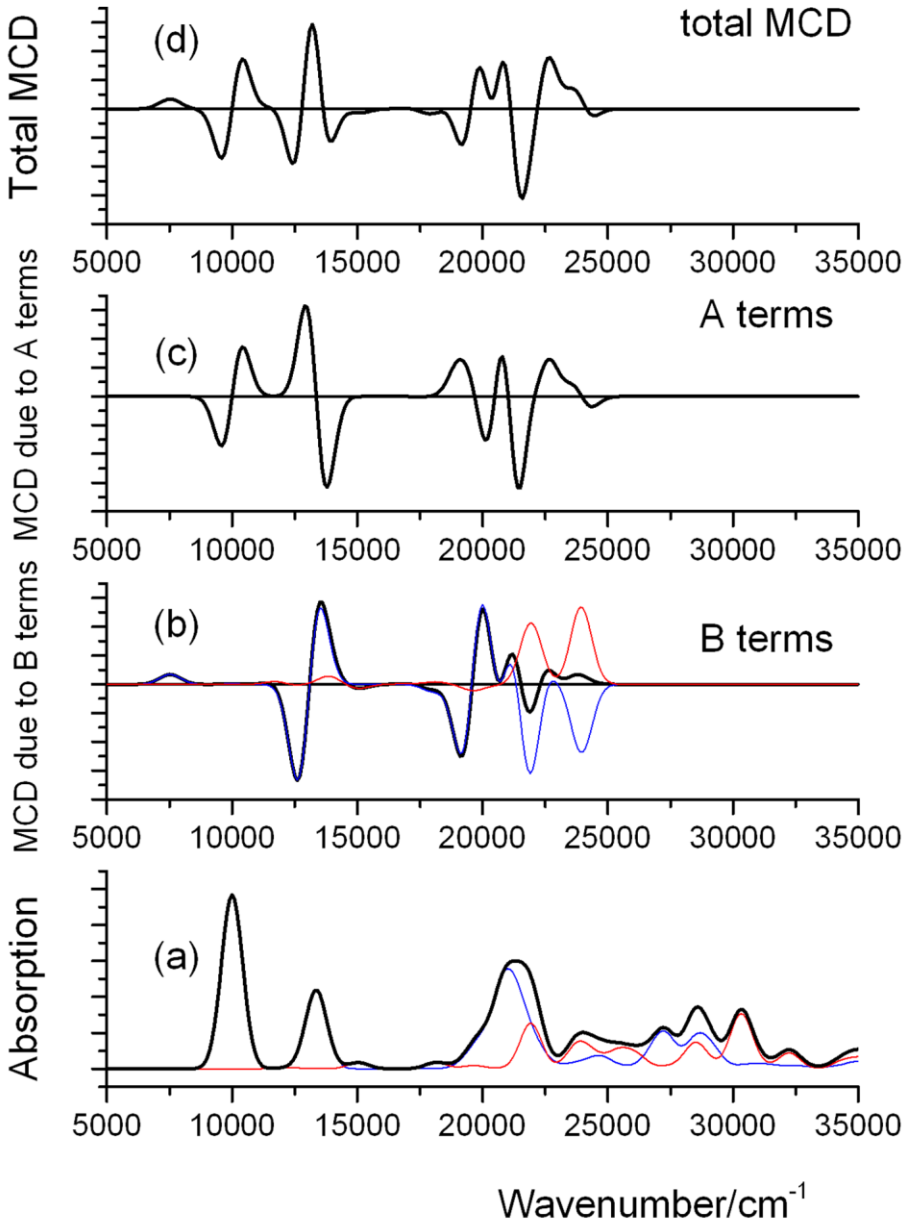

Figure 8. Calculated absorption (a) and MCD spectra (d) of "rigid" ***c*-P6**. (b) and (c), contributions from *B* and *A* terms, respectively, to the total MCD signal. Blue and red, contributions from E_{1u} and A_{2u} transitions, respectively.

References

1. J. Michl, *Tetrahedron*, 1984, **40**, 3845-3934.
2. J. D. Keegan, A. M. Stolzenberg, Y. C. Lu, R. E. Linder, G. Barth, E. Bunnenberg, C. Djerassi and A. Moscowitz, *J. Am. Chem. Soc.*, 1981, **103**, 3201-3203.
3. J. D. Keegan, A. M. Stolzenberg, Y. C. Lu, R. E. Linder, G. Barth, A. Moscowitz, E. Bunnenberg and C. Djerassi, *J. Am. Chem. Soc.*, 1982, **104**, 4305-4317.
4. J. D. Keegan, A. M. Stolzenberg, Y. C. Lu, R. E. Linder, G. Barth, A. Moscowitz, E. Bunnenberg and C. Djerassi, *J. Am. Chem. Soc.*, 1982, **104**, 4317-4329.
5. R. A. Goldbeck, B. R. Tolf, A. G. H. Wee, A. Y. L. Shu, R. Records, E. Bunnenberg and C. Djerassi, *J. Am. Chem. Soc.*, 1986, **108**, 6449-6458.
6. R. A. Goldbeck, B. R. Tolf, E. Bunnenberg and C. Djerassi, *J. Am. Chem. Soc.*, 1987, **109**, 28-32.
7. M. N. Glukhovstev, A. Pross, M. P. McGrath and L. Radom, *J. Chem. Phys.*, 1995, **103**, 1878-1885.
8. N. Kobayashi and K. Nakai, *Chem. Commun.*, 2007, 4077-4092.
9. J. Mack, M. J. Stillman and N. Kobayashi, *Coord. Chem. Rev.*, 2007, **251**, 429-453.
10. J. Mack, *Chem. Rev.*, 2017, **117**, 3444-3478.
11. S. Sripothongnak, C. J. Ziegler, M. R. Dahlby and V. N. Nemykin, *Inorg. Chem.*, 2011, **50**, 6902-6909.
12. C. J. Ziegler, N. R. Erickson, M. R. Dahlby and V. N. Nemykin, *J. Phys. Chem. A*, 2013, **117**, 11499-11508.
13. S. Doble, A. J. Osinski, S. M. Holland, J. M. Fisher, G. R. Geier, R. V. Belosludov, C. J. Ziegler and V. N. Nemykin, *J. Phys. Chem. A*, 2017, **121**, 3689-3698.
14. J. L. Shaw, S. J. Doble, J. Stewart and V. N. Nemykin, *J. Porphyrins Phthalocyanines*, 2017, **21**, 287-294.
15. J. Yan, Y. Yang, M. Ishida, S. Mori, B. Zhang, Y. Feng and H. Furuta, *Chem. - Eur. J.*, 2017, **23**, 11375-11384.
16. V. N. Nemykin, G. T. Rohde, C. D. Barrett, R. G. Hadt, J. R. Sabin, G. Reina, P. Galloni and B. Floris, *Inorg. Chem.*, 2010, **49**, 7497-7509.
17. Y. Saegusa, T. Ishizuka, K. Komamura, S. Shimizu, H. Kotani, N. Kobayashi and T. Kojima, *Phys. Chem. Chem. Phys.*, 2015, **17**, 15001-15011.
18. S. Sugawara, Y. Hirata, S. Kojima, Y. Yamamoto, E. Miyazaki, K. Takimiya, S. Matsukawa, D. Hashizume, J. Mack, N. Kobayashi, Z. Fu, K. M. Kadish, Y. M. Sung, K. S. Kim and D. Kim, *Chem. - Eur. J.*, 2012, **18**, 3566-3581, S3566/3561-S3566/3522.
19. T. Yoshida, W. Zhou, T. Furuyama, D. B. Leznoff and N. Kobayashi, *J. Am. Chem. Soc.*, 2015, **137**, 9258-9261.
20. Y. Yu, T. Furuyama, J. Tang, Z.-Y. Wu, J.-Z. Chen, N. Kobayashi and J.-L. Zhang, *Inorg. Chem. Front.*, 2015, **2**, 671-677.
21. C. J. Ziegler, J. R. Sabin, G. R. Geier and V. N. Nemykin, *Chem. Commun. (Cambridge, U. K.)*, 2012, **48**, 4743-4745.
22. H. M. Rhoda, L. A. Crandall, G. R. Geier, III, C. J. Ziegler and V. N. Nemykin, *Inorg. Chem.*, 2015, **54**, 4652-4662.
23. X. Liang, Y. Niu, Q. Zhang, J. Mack, X. Yi, Z. Hlatshwayo, T. Nyokong, M. Li and W. Zhu, *Dalton Trans.*, 2017, **46**, 6912-6920.
24. T. Ito, Y. Hayashi, S. Shimizu, J.-Y. Shin, N. Kobayashi and H. Shinokubo, *Angew. Chem., Int. Ed.*, 2012, **51**, 8542-8545, S8542/8541-S8542/8514.
25. D. Caldwell, J. M. Thorne and H. Eyring, *Annu. Rev. Phys. Chem.*, 1971, **22**, 259-278.
26. J. Michl, *J. Am. Chem. Soc.*, 1978, **100**, 6801-6811.

27. J. Michl, *J. Am. Chem. Soc.*, 1978, **100**, 6812-6818.
28. J. Michl, *J. Am. Chem. Soc.*, 1978, **100**, 6819-6824.
29. M. Gouterman, *J. Chem. Phys.*, 1959, **30**, 1139-1161.
30. M. Gouterman, *J. Mol. Spectrosc.*, 1961, **6**, 138-163.
31. A. Muranaka, O. Matsushita, K. Yoshida, S. Mori, M. Suzuki, T. Furuyama, M. Uchiyama, A. Osuka and N. Kobayashi, *Chem. - Eur. J.*, 2009, **15**, 3744-3751.
32. N. Toriumi, A. Muranaka, E. Kayahara, S. Yamago and M. Uchiyama, *J. Am. Chem. Soc.*, 2015, **137**, 82-85.
33. J. Fleischhauer and J. Michl, *J. Phys. Chem. A*, 2000, **104**, 7776-7784.
34. J. Fleischhauer, U. Höweler, J. Spanget-Larsen, G. Raabe and J. Michl, *J. Phys. Chem. A*, 2004, **108**, 3225-3234.
35. J. Fleischhauer, G. Raabe, K. A. Klingensmith, U. Howeler, P. K. Chatterjee, K. Hafner, E. Vogel and J. Michl, *Int. J. Quantum Chem.*, 2005, **102**, 925-939.
36. J. Waluk, M. Müller, P. Swiderek, M. Köcher, E. Vogel, G. Hohlneicher and J. Michl, *J. Am. Chem. Soc.*, 1991, **113**, 5511-5527.
37. A. Gorski, E. Vogel, J. L. Sessler and J. Waluk, *J. Phys. Chem. A*, 2002, **106**, 8139-8145.
38. A. Gorski, E. Vogel, J. L. Sessler and J. Waluk, *Chem. Phys.*, 2002, **282**, 37-49.
39. A. Gorski, T. Köhler, D. Seidel, J. T. Lee, G. Orzanowska, J. L. Sessler and J. Waluk, *Chem.-Eur. J.*, 2005, **11**, 4179-4184.
40. J. Waluk and J. Michl, *Inorg. Chem.*, 1981, **20**, 963-965.
41. M. Hoffmann, J. Kärnbratt, M. H. Chang, L. M. Herz, B. Albinsson and H. L. Anderson, *Angew Chem Int Edit*, 2008, **47**, 4993-4996.
42. J. K. Sprafke, D. V. Kondratuk, M. Wykes, A. L. Thompson, M. Hoffmann, R. Drevinskas, W. H. Chen, C. K. Yong, J. Karnbratt, J. E. Bullock, M. Malfois, M. R. Wasielewski, B. Albinsson, L. M. Herz, D. Zigmantas, D. Beljonne and H. L. Anderson, *J. Am. Chem. Soc.*, 2011, **133**, 17262-17273.
43. M. G. Gatty, A. Kahnt, L. J. Esdaile, M. Hutin, H. L. Anderson and B. Albinsson, *J. Phys. Chem. B*, 2015, **119**, 7598-7611.
44. B. Albinsson and H. L. Anderson, in *Multiporphyrin Arrays: Fundamentals and Applications*, 2012, DOI: Book_Doi 10.1201/B11621, pp. 55-90.
45. G. Sedghi, V. M. Garcia-Suarez, L. J. Esdaile, H. L. Anderson, C. J. Lambert, S. Martin, D. Bethell, S. J. Higgins, M. Elliott, N. Bennett, J. E. Macdonald and R. J. Nichols, *Nat Nanotechnol*, 2011, **6**, 517-523.
46. P. Parkinson, C. E. I. Knappke, N. Kamonsutthipaijit, K. Sirithip, J. D. Matichak, H. L. Anderson and L. M. Herz, *J. Am. Chem. Soc.*, 2014, **136**, 8217-8220.
47. C. K. Yong, P. Parkinson, D. V. Kondratuk, W. H. Chen, A. Stannard, A. Summerfield, J. K. Sprafke, M. C. O'Sullivan, P. H. Beton, H. L. Anderson and L. M. Herz, *Chem. Sci.*, 2015, **6**, 181-189.
48. M. H. Chang, M. Hoffmann, H. L. Anderson and L. M. Herz, *J. Am. Chem. Soc.*, 2008, **130**, 10171-10178.
49. F. V. D. Camargo, L. Grimmelsmann, H. L. Anderson, S. R. Meech and I. A. Heisler, *Phys. Rev. Lett.*, 2017, **118**, 033001.
50. J. D. Wilkinson, G. Wicks, A. Nowak-Król, L. G. Łukasiewicz, C. J. Wilson, M. Drobizhev, A. Rebane, D. T. Gryko and H. L. Anderson, *J. Mat. Chem. C*, 2014, **2**, 6802-6809.
51. M. Drobizhev, Y. Stepanenko, A. Rebane, C. J. Wilson, T. E. O. Screen and H. L. Anderson, *J. Am. Chem. Soc.*, 2006, **128**, 12432-12433.
52. S. Richert, J. Cremers, I. Kuprov, M. D. Peeks, H. L. Anderson and C. R. Timmel, *Nat. Comm.*, 2017, **8**.
53. V. Butkus, J. Alster, E. Baginskaite, R. Augulis, P. Neuhaus, L. Valkunas, H. L. Anderson, D. Abramavicius and D. Zigmantas, *J. Phys. Chem. Lett.*, 2017, **8**, 2344-2349.

54. M. D. Peeks, T. D. W. Claridge and H. L. Anderson, *Nature*, 2017, **541**, 200-203.
55. J. D. Keegan, E. Bunnenberg and C. Djerassi, *Spectrochim. Acta, Part A*, 1984, **40A**, 287-297.
56. P. N. Taylor, J. Huuskonen, G. Rumbles, R. T. Aplin, E. Williams and H. L. Anderson, *Chem. Commun.*, 1998, DOI: , 909-910.
57. A. McHugh, M. Gouterman and C. J. Weiss, *Theor. Chim. Acta*, 1972, **24**, 346-370.
58. M. Gilbert, L. J. Esdaile, M. Hutin, K. Sawada, H. L. Anderson and B. Albinsson, *J Phys Chem C*, 2013, **117**, 26482-26492.
59. F. V. A. Camargo, H. L. Anderson, S. R. Meech and I. A. Heisler, *J. Phys. Chem. B*, 2015, **119**, 14660-14667.
60. F. V. A. Camargo, C. R. Hall, H. L. Anderson, S. R. Meech and I. A. Heisler, *Struct. Dyn.*, 2016, **3**, 023608-023601-023612.
61. M. D. Peeks, P. Neuhaus and H. L. Anderson, *Phys. Chem. Chem. Phys.*, 2016, **18**, 5264-5274.
62. M. U. Winters, J. Karnbratt, H. E. Blades, C. J. Wilson, M. J. Frampton, H. L. Anderson and B. Albinsson, *Chem-Eur J*, 2007, **13**, 7385-7394.
63. M. U. Winters, J. Karnbratt, M. Eng, C. J. Wilson, H. L. Anderson and B. Albinsson, *J. Phys. Chem. C*, 2007, **111**, 7192-7199.
64. G. A. Peralta, M. Seth and T. Ziegler, *Inorg. Chem.*, 2007, **46**, 9111-9125.
65. H. Solheim, K. Ruud, S. Coriani and P. Norman, *J. Phys. Chem. A*, 2008, **112**, 9615-9618.
66. J. Mack, Y. Asano, N. Kobayashi and M. J. Stillman, *J. Am. Chem. Soc.*, 2005, **127**, 17697-17711.
67. W. R. Scheidt, J. U. Mondal, C. W. Eigenbrot, A. Adler, L. J. Radonovich and J. L. Hoard, *Inorg. Chem.*, 1986, **25**, 795-799.
68. U. Even, J. Magen, J. Jortner, J. Friedman and H. Levanon, *J. Chem. Phys.* , 1982, **77**, 4374-4383.
69. C. E. Tait, P. Neuhaus, H. L. Anderson and C. R. Timmel, *J. Am. Chem. Soc.*, 2015, **137**, 6670-6679.
70. M. Drobizhev, Y. Stepanenko, Y. Dzenis, A. Karotki, A. Rebane, P. N. Taylor and H. L. Anderson, *J. Phys. Chem. B*, 2005, **109**, 7223-7236.
71. H. L. Anderson, *Inorg. Chem.*, 1994, **33**, 972-981.
72. S. Ohira and J. L. Bredas, *J. Mater. Chem.*, 2009, **19**, 7545-7550.
73. R. V. Belosludov, H. M. Rhoda, R. K. Zhdanov, V. R. Belosludov, Y. Kawazoe and V. N. Nemykin, *Phys. Chem. Chem. Phys.*, 2016, **18**, 13503-13518 (Erratum Phys. Chem. Chem. Phys., 2017, 13519, 20290).
74. M. D. Peeks, C. E. Tait, P. Neuhaus, G. M. Fischer, M. Hoffmann, R. Haver, A. Cnossen, J. R. Harmer, C. R. Timmel and H. L. Anderson, *J. Am. Chem. Soc. 2017, doi 10.1021/jacs.7b05386*
75. C. E. Tait, P. Neuhaus, M. D. Peeks, H. L. Anderson and C. R. Timmel, *J. Am. Chem. Soc.*, 2015, **137**, 8284-8293.
76. G. te Velde, F. M. Bickelhaupt, E. J. Baerends, C. Fonseca Guerra, S. J. A. van Gisbergen, J. G. Snijders and T. Ziegler, *J. Comput. Chem.*, 2001, **22**, 931-967.
77. C. Fonseca Guerra, J. G. Snijders, G. te Velde and E. J. Baerends, *Theor. Chem. Acc.*, 1998, **99**, 391-403.
78. M. Seth and T. Ziegler, *J. Chem. Phys.*, 2007, **127**, 134108.
79. M. Seth, M. Krykunov, T. Ziegler, J. Autschbach and A. Banerjee, *J. Chem. Phys.*, 2008, **128**, 144105.
80. M. Seth, M. Krykunov, T. Ziegler and J. Autschbach, *J. Chem. Phys.*, 2008, **128**, 234102.
81. A. D. Becke, *Phys. Rev. A*, 1988, **38**, 3098-3100.
82. J. P. Perdew, *Phys. Rev. B*, 1986, **33**, 8822-8824 (Erratum PRB 88*34*, 1986, 7406).